Dynamic local distortions in $KNbO_3$

1999 J. Phys.: Condens. Matter 11 3779

(http://iopscience.iop.org/0953-8984/11/18/313)

J. Phys.: Condens. Matter **11** (1999) 3779–3787. Printed in the UK PII: S0953-8984(99)02282-1

Dynamic local distortions in $KNbO_3$

Henry Krakauer†, Rici Yu†§, Cheng-Zhang Wang†, Karin M Rabe‡ and Umesh V Waghmare‡‖

† Department of Physics, College of William and Mary, Williamsburg, VA 23187-8795, USA
‡ Yale University, Department of Applied Physics, PO Box 208284, New Haven, CT 06520-8284, USA

Received 5 March 1999

Abstract. Molecular dynamics simulations of the perovskite oxide $KNbO_3$ are performed with a first-principles effective Hamiltonian. They reveal the prevalence of local polar distortions with short-range chain-like correlations, present even in the paraelectric phase far above T_c. The ordering of these dynamically fluctuating distortions yields the observed temperature sequence of ferroelectric phases. The simulations also reproduce the essential features of diffuse x-ray scattering measurements and the weak temperature dependence of diffuse streak patterns observed by Comes *et al*. These local distortions suggest an order–disorder character for the transitions. Softening of optical phonon branches is observed in the same simulations not only near $q = 0$, suggesting a displacive character for the transition, but also over large regions of the Brillouin zone. Dynamic real-space chains thus provide a unified framework for understanding both the order–disorder and displacive characteristics of these phase transitions.

1. Introduction

There are many experimental indications in perovskite ferroelectrics that the actual atomic structure in some of the phases may be significantly different locally to that indicated by the average crystallographic structure deduced from elastic x-ray and neutron scattering. Diffuse x-ray scattering measurements of Comes *et al* [1,2] on the temperature-dependent paraelectric and ferroelectric phases of $KNbO_3$ and $BaTiO_3$ revealed phase-dependent streak patterns well above the ferroelectric transition temperatures. These patterns were interpreted as evidence for short-range order in the form of a *static* chain structure. Other observations such as quasi-elastic central peaks in neutron scattering [3] and Raman spectroscopy [4] above the phase transition temperature are also indicative of preformed clusters of the low-temperature phase. More recently, pair distribution functions obtained from neutron scattering measurements up to very high momentum transfers [5] and XAFS measurements [6] indicate the presence of local distortions with short-range order. These local distortions suggest an order–disorder character for the observed phase transitions. On the other hand, there is extensive evidence supporting a displacive mechanism for the transitions, as indicated by the $q = 0$ Curie–Weiss softening of transverse optic (TO) phonon modes. However, in a displacive phase transition, local distortions are expected to disappear rapidly above T_c.

First-principles calculations provide a powerful tool for the detailed microscopic investigation of atomic geometry and structural instabilities. In previous work [7] using the

§ Present address: General Sciences Corporation, Laurel, MD 20707, USA.
‖ Present address: Department of Physics, Harvard University, Cambridge, MA 02138, USA.

0953-8984/99/183779+09$19.50

LAPW linear response method for the calculation of the zero-temperature phonon dispersion in the cubic perovskite structure, the instability of $KNbO_3$ against the formation of localized chain distortions was observed. Similar calculations subsequently established the same instability for $BaTiO_3$ [8]. However, these investigations were limited to zero temperature and to relatively small simulation cells. Thus the implications of these results for static or dynamical structural distortions and phonons at non-zero temperature could not be determined.

With the construction of an effective Hamiltonian, the reach of the first-principles results can be greatly extended. This has already proved to be a useful strategy for the quantitative analysis of temperature-driven structural phase transitions in real materials [9–12]. The effective Hamiltonian acts in the subspace of the full ionic configuration space which contains the degrees of freedom relevant to the transition(s). These include, in particular, the 'soft mode', identified as the unstable mode of the high-symmetry structure which freezes in to produce the low-symmetry phase(s). In this subspace, the Born–Oppenheimer surface is written as a Taylor expansion about the high-symmetry structure. The expansion coefficients are determined from first-principles total-energy and linear response results, eliminating the need for empirical input. Given certain approximations, non-zero-temperature simulations using H_{eff} then should exactly reproduce the transition behaviour, with generic underestimates of calculated T_cs being attributable to the use of the local density approximation, neglect of higher-order coupling to degrees of freedom outside the effective-Hamiltonian subspace, and the sensitivity of the transition to residual inaccuracies in the parametrization of strain coupling.

In this paper, a complementary analysis of the temperature dependence of both the real-space distortions and the optic phonon branches throughout the Brillouin zone is performed with a first-principles effective-Hamiltonian molecular dynamics method. In section 2, we describe the construction of the effective Hamiltonian for $KNbO_3$ and the method used for the classical molecular dynamics simulations. In section 3, we present the results of calculations of system averages and intersite correlations first in real space and then in reciprocal space, showing that the phase sequence, the existence of preformed real-space chains, the diffuse x-ray patterns, and the softening of $q = 0$ phonons are all well reproduced, accounting for both the order–disorder and displacive aspects of the ferroelectric transitions. Section 4 concludes the paper.

2. Methodology

We constructed H_{eff} for $KNbO_3$ using the lattice Wannier-function (LWF) method [11]. Full details of the construction are presented elsewhere [13], and we give only a brief description here. The effective-Hamiltonian subspace is defined using a basis of localized and symmetrized atomic displacement patterns, called lattice Wannier functions, which are constructed to reproduce the first-principles unstable polar Γ_{15} phonon as well as unstable transverse optic phonon eigenvectors and frequencies at other high-symmetry points in the BZ [7]. For $KNbO_3$, the subspace is spanned by one vector degree of freedom per unit cell, $\xi_{i\alpha}$, representing the LWF coordinates, where i = unit-cell index and $\alpha = x, y, z$. We include as additional degrees of freedom the homogeneous strain tensor, which describes changes in the overall volume and shape of the simulation cell.

In the LWF basis, the kinetic energy retains a simple diagonal form. The potential energy is expressed as a Taylor expansion in the LWF coordinates $\xi_{i\alpha}$ and can be organized as follows:

$$U = U_{\text{on-site}} + U_{\text{short-range}} + U_{\text{dipolar}} + U_{\text{LWF-strain}} + U_{\text{elastic}}. \tag{1}$$

We include anharmonic terms only in the on-site interaction

$$U_{\text{on-site}} = \kappa \xi_i^2 + \delta \xi_i^4 + \gamma (\xi_{ix}^2 \xi_{iy}^2 + \text{c.p.})$$

and in the lowest-order coupling between LWF coordinates (on-site quadratic) and homogeneous strain (linear) $U_{\mathrm{LWF-strain}}$. Strain coupling of this type has been shown to be crucial in obtaining the experimentally observed sequence of ferroelectric phase transitions in perovskite ferroelectrics [10,14]. The coefficients of the on-site anharmonic and strain coupling terms were determined by fitting to first-principles total energies, varying the strain and amplitude of uniform LWF distortions in the [100], [110] and [111] directions. The interactions between LWF coordinates in different unit cells are included to quadratic order only, with the general form $\sum_{ij\alpha\beta} J_{ij\alpha\beta}\xi_{i\alpha}\xi_{j\beta}$. Beyond third neighbours, the $J_{ij\alpha\beta}$ are parametrized as the interaction between two dipoles $Z^*\vec{\xi}_i$ and $Z^*\vec{\xi}_j$, where Z^* is the mode effective charge for the unstable zone-centre phonon, screened by the electronic dielectric constant ε_∞. Z^* and ε_∞ are computed directly using LAPW linear response, while the short-range $J_{ij\alpha\beta}$ are fitted to the first-principles dynamical-matrix elements.

Using H_{eff}, classical molecular dynamics simulations were carried out for a $10 \times 10 \times 10$ simulation cell, corresponding to 5000 atoms, with periodic boundary conditions; the $\xi_{i\alpha}$ in H_{eff} are in units of $a/10$, where $a = 4.016$ Å is the lattice constant. A variable cell shape formalism was used together with Nosé–Hoover thermostats to equilibrate the MD runs at constant temperature [15]. After equilibration, and prior to computing the static and dynamic structure factors, the thermostats were turned off and the cell shape and volume were kept fixed. Further equilibration (constant-energy MD) generally caused the temperature to change by about 5 K. After this last equilibration, MD runs of typically 20 000 time steps (each time step $\sim$ one femtosecond) were performed. The static and dynamic structure factors and spectral density $S_{\xi\xi}(q,\omega)$ of the $\xi_{i\alpha}$ were then computed [16] using data from every tenth time step.

3. Results and discussion

The various structural phases and transition temperatures T_c are identified in the MD simulations by calculating the three components of the order parameter S_α, defined as an average over the LWF coordinates: $S_\alpha = (1/N)\sum_i \xi_{i\alpha}$. For example, the time average of all three components of the order parameter is zero at 400 K in $KNbO_3$, indicating that the system is in the cubic paraelectric phase. At 370 K, one of the components of the order parameter freezes out with a non-zero average value of about 0.16, but the time average of the other two components is still zero, indicating that the system is in the tetragonal phase. Subsequent freezing out of the other components signals transitions to the orthorhombic and rhombohedral phases. The MD T_c-values were calculated by us for $KNbO_3$ and, as a calibration of the method, for $BaTiO_3$, using the H_{eff} constructed in reference [10]. The results, given in table 1, are averages of cooling and heating runs, and we estimate the error in these numbers to be about 5–10 K. As mentioned, the calculated T_c for the cubic–tetragonal transition is significantly underestimated for both materials. T_cs for the R–O and O–T transitions are in better agreement, with the R–O agreement being the best. In any case, the non-trivial phase sequence and the trend from $BaTiO_3$ to $KNbO_3$ are correctly reproduced, suggesting that the effective Hamiltonian captures the essential behaviour of the microscopic fluctuations driving the transitions.

First, we interpret experimental observations of local distortions and short-range order by analysing the simulation results in real space. Figure 1 shows the time dependence in $KNbO_3$ of the real-space LWF coordinates for three cases: (1) ξ_{iy} in the 230 K orthorhombic phase (lowest family of curves), (2) ξ_{ix} in the 230 K orthorhombic phase (middle family of curves), and (3) ξ_{ix} in the 390 K cubic phase (uppermost family of curves). Each family of curves consists of six curves, ($i = 0, \ldots, 5$) for LWF coordinate components in six adjacent

Table 1. Comparison of calculated and measured transition temperatures (see the text), between the rhombohedral (R), orthorhombic (O), tetragonal (T), and cubic (C) phases. Temperatures are in kelvin.

	R–O	O–T	T–C
$KNbO_3$			
MD	210	260	370
Experiment[a]	210–265	488	701
$BaTiO_3$			
MD	200	230	290
MC[b]	197	230	290
Experiment[c]	183	278	403

[a] See, for example, reference [21].
[b] Reference [10].
[c] From reference [10].

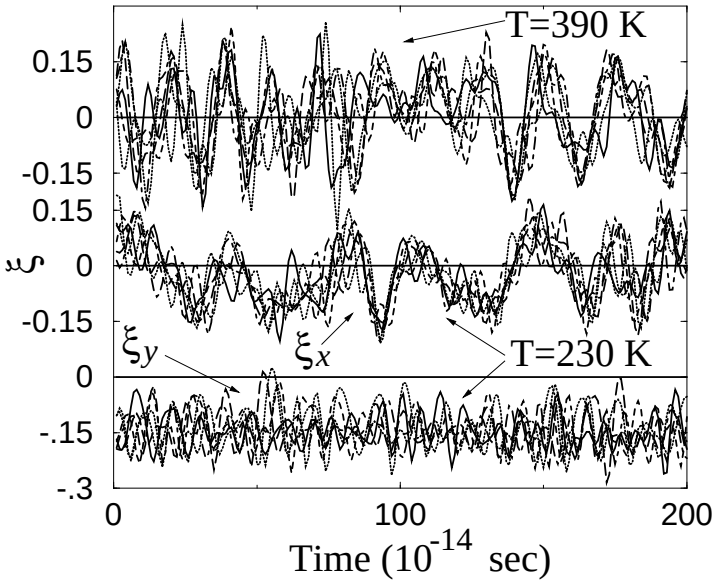

Figure 1. The time dependence of the LWF coordinate components ξ_{ix} and ξ_{iy} in the orthorhombic (230 K) and cubic (390 K) phases of $KNbO_3$, for six ($i = 0, \ldots, 5$) adjacent primitive cells along an uncondensed chain in the x-direction (see the text). The order parameters S_y and S_z are condensed, but $S_x = 0$. Chain-like correlations are evident in the correlated motion of the six LWF coordinates ξ_{ix} as a function of time, but not in the y-components, which oscillate randomly about the condensed value of -0.16.

primitive cells along the x-direction, i.e. along a [100] 'chain'. The x-direction was chosen because the order parameter S_x was zero or 'uncondensed' in all of the simulations shown. All components of the order parameter are zero in the cubic phase, of course, but in the orthorhombic phase, the S_y- and S_z-components were non-zero or 'condensed'. There is a dramatic difference between the lower and middle family of curves, both of which are for the 230 K orthorhombic phase. The lower family shows that the LWF components giving displacements in the y-direction, ξ_{iy}, are uncorrelated for adjacent cells along the x-direction. (Note that the average value is non-zero, corresponding to the condensed S_y order parameter.) There is also no correlation between adjacent x-chains of the ξ_{ix}-displacements (not shown).

By contrast, the middle family of curves shows that the LWF components ξ_{ix}, displacements along the x-chain, are strongly correlated along the x-direction. The same correlation between the ξ_{ix} is observed in the upper family of curves for the cubic phase. The order parameter component $S_x = (1/N)\sum_i \xi_{ix}$ measures the long-range order associated with the ξ_{ix}-displacements. Although S_x is zero on average, figure 1 shows that there is *dynamic* chain-like short-range order present in the system, with the characteristic chain-reversal frequency increasing with increasing temperature. In the cubic phase the chain correlations persist to temperatures far above the cubic–tetragonal ferroelectric phase transition, and we also observe (not shown) identical correlated ξ_{iy}-displacements for adjacent cells in the y-direction, and for ξ_{iz}-displacements along the z-direction.

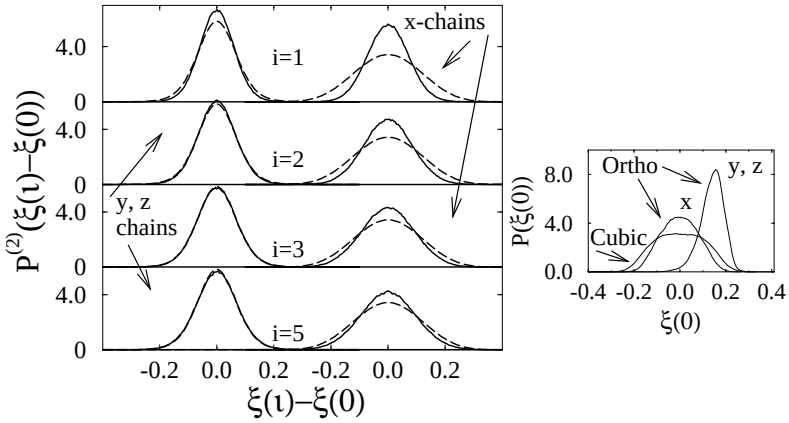

Figure 2. The solid curves are two-site equal-time probability distributions, $P^{(2)}(\xi(i) - \xi(0))$, for $i = 1$, 2, 3, and 5 along condensed y- and z-chains and for uncondensed x-chains in orthorhombic $KNbO_3$. In both cases, ξ represents the longitudinal component of the LWF coordinate along the chain direction. The dashed curves are obtained using the one-site probability distribution, assuming no correlation between the two sites. The inset shows the one-site probability distributions, $P(\xi(0))$, for the x-, y-, and z-components in the orthorhombic phase, as well as in the cubic phase. (Due to the use of periodic boundary conditions in the $10 \times 10 \times 10$ simulation cell, the largest nearest-neighbour distance along a chain is $5a$.)

Figure 2 gives a more quantitative account of these correlated motions. The inset shows the one-site probability distributions, $P(\xi(0))$, for the x-, y-, and z-components in the orthorhombic phase, as well as in the cubic phase. Since the y- and z-components of the order parameter are condensed in the orthorhombic phase, their respective distributions are not centred on zero, while the x-distribution is centred on zero in both the orthorhombic and cubic phases. Moreover, the y- and z-distributions are narrower than the x-distribution. Due to its higher temperature, the x-distribution in the cubic phase is broader than that in the orthorhombic phase. The main figure presents two-site equal-time probability distributions for the orthorhombic phase of $KNbO_3$, $P^{(2)}(\xi(i) - \xi(0))$, for longitudinal displacements along chains, with $i = 1$, 2, 3, and 5 indexing primitive cells along condensed y- and z-chains (curves on the left) and for uncondensed x-chains (curves on the right). In both cases, the dashed curves are obtained using the one-site probability distributions shown in the inset and assuming that there is no correlation between the two sites. The large differences between the dashed and solid $P^{(2)}(\xi(i) - \xi(0))$ curves on the right reflects the ξ_{ix} chain-like correlations along x-chains. The dashed and solid curves on the left, however, are almost indistinguishable, indicating no longitudinal correlations along the condensed y- and z-chains.

Next, we show that the dynamic chain-like correlations that we have found in $KNbO_3$

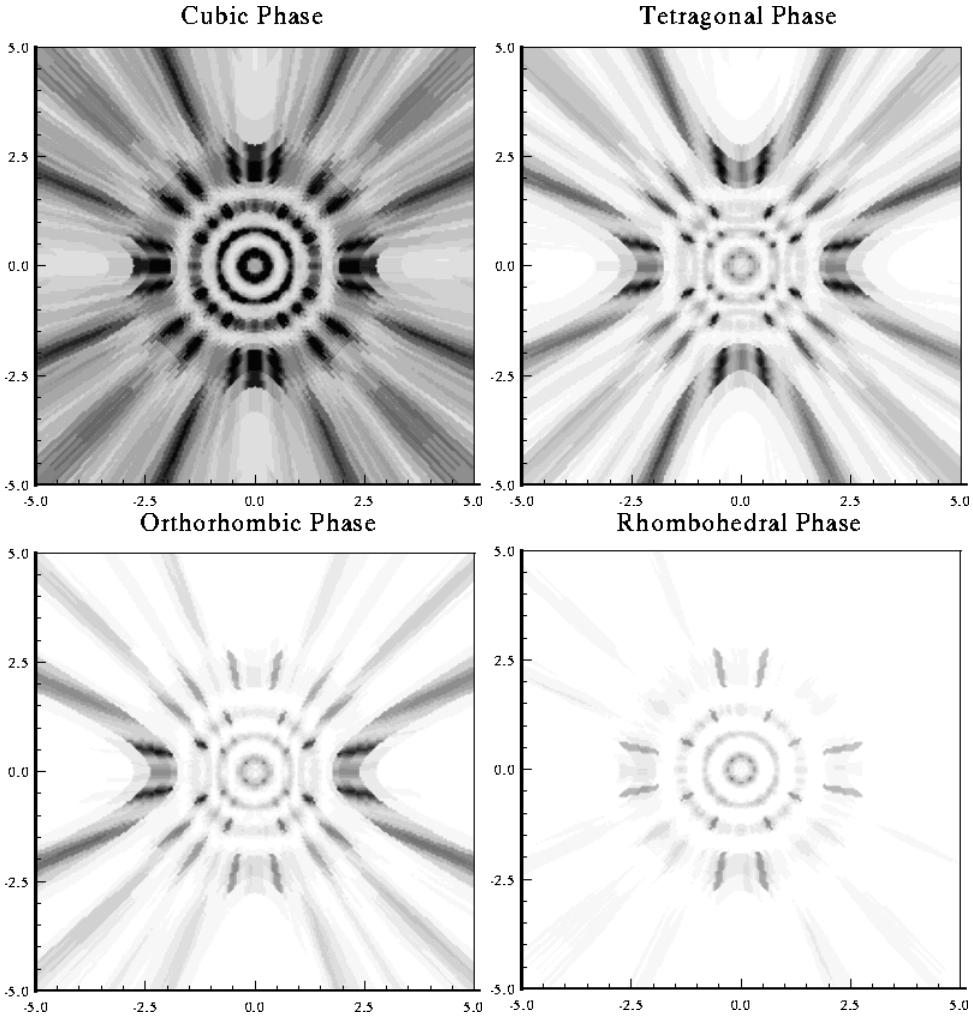

Figure 3. Calculated diffuse x-ray scattering in $BaTiO_3$, corresponding to monochromatic Mo Kα (see the text). The plane of the figure is perpendicular to a cubic axis and to the incident x-ray. (a) cubic, (b) tetragonal, (c) orthorhombic, and (d) rhombohedral phases.

and $BaTiO_3$ are consistent with the observed diffuse x-ray scattering intensity streak patterns. Figure 3 presents simulated diffuse elastic x-ray scattering intensities. These were determined from static-structure-factor $S(q)$ MD calculations for $BaTiO_3$ [18]. The position and sequential disappearance of the three families (circles, vertical, and horizontal, respectively) of streak patterns on cooling from the cubic to rhombohedral phases reproduces the behaviour observed in $BaTiO_3$ and $KNbO_3$ [2]. Moreover, the streak intensities are only slowly varying functions of temperature within a structural phase and persist well above the cubic-to-tetragonal transition. To explain the streak patterns, Comes *et al* invoked scattering from disordered finite-length static chains, hypothesizing that upon cooling there is a sequential ordering of chains directed along the three cubic axes. Thus, for example, in the cubic-to-tetragonal transition, the ordering of the z-chains corresponds to the disappearance of the incoherent scattering (circular streaks in figure 6(a) of reference [2]) due to randomly oriented z-chains. Subsequent ordering of the

x- and y-chains corresponds to entering the orthorhombic and rhombohedral phases, with all of the chains being ordered in the ground-state rhombohedral phase. In further work, Hüller [20] alternatively proposed that the streak patterns could be explained dynamically. More recently, Holma *et al* [19] performed a careful analysis of their diffuse x-ray measurements and concluded that their results were in better agreement with Holma's model of dynamic chains. The *ab initio* linear response calculations of Yu and Krakauer [7] on $KNbO_3$ and of Ghosez *et al* [8] on $BaTiO_3$ provided theoretical support for both of these explanations by showing the existence of BZ slab-like instabilities, which could result in either static or dynamic chains. The present MD simulations, which use an H_{eff} based on the first-principles results, conclusively show that the chains are dynamic, and figure 3 shows that these dynamic chains can also reproduce the diffuse x-ray data.

The local distortions and short-range order on short length scales in real space imply that the structural instability occurs over large regions in wavevector space. At zero temperature, this correspondence has been observed in the *ab initio* linear response calculations of Yu and Krakauer [7] on $KNbO_3$ and of Ghosez *et al* [8] on $BaTiO_3$, which revealed unstable (i.e. imaginary-frequency) TO branches extending all the way out to the BZ boundaries along $\langle 100 \rangle$ directions and throughout three mutually perpendicular interpenetrating slabs centred at $q = 0$. In the high-temperature phases, this suggests the possibility of the softening of entire anharmonically stabilized phonon branches.

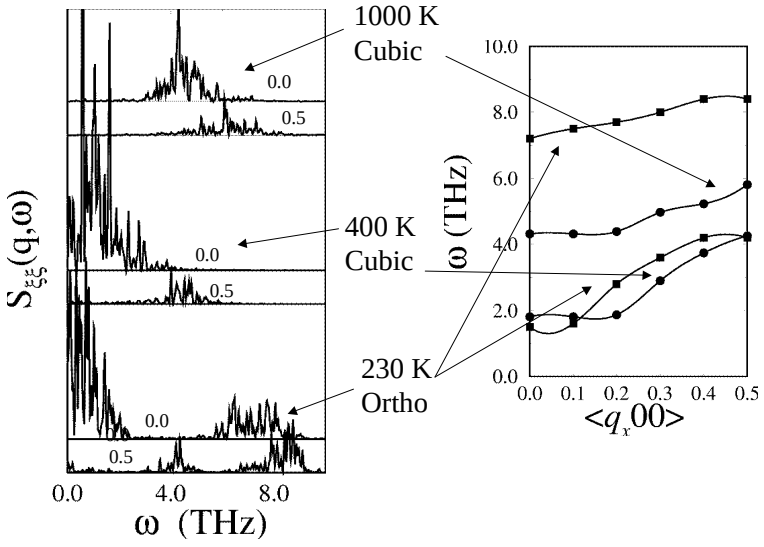

Figure 4. Left-hand panel: $S_{\xi\xi}(q, \omega)$ for $q = [000]$ and $[0.5\,0\,0]$ at three temperatures. The degeneracy of the TO modes in the cubic phase is lifted in the orthorhombic phase. Right-hand panel: the full [100] wavevector dependence of the TO $S_{\xi\xi}(q, \omega)$ peak positions.

In our MD simulations for $KNbO_3$, the temperature-dependent phonon dispersion was determined from the wavevector dependence of pronounced peaks in the Fourier-transformed autocorrelation function. The left-hand panel of figure 4 shows examples of the calculated spectral density $S_{\xi\xi}(q, \omega)$ [16], for three different temperatures, at reduced wavevectors $q = 0.0$ and 0.5, and the right-hand panel shows the full dispersion of these peaks for all wavevectors along the [100] direction in the Brillouin zone. These results are characterized by well-defined phonon peaks, identified as TO modes. The two TO branches are degenerate in the cubic phase, but split in the orthorhombic phase with one being stiffened dramatically

to higher frequency. The frequency for small q in the cubic phase at $T = 400$ K (30 K above T_c) is in good agreement with the TO frequency measured through inelastic neutron scattering by Holma and Chen [17] about 100 K above the transition. For larger wavevectors, the experimentally deduced dispersion is considerably flatter than that calculated, but the precise dispersion for $q \geqslant 0.3$ may be somewhat uncertain, because the measured peak intensity was extremely low and the background unusually high.

The most striking feature of figure 4 is that the *entire* TO branch is very much temperature dependent. This behaviour differs from the usual picture of a displacive transition, in which softening occurs only in the vicinity of the wavevector associated with the structural phase transition ($q = 0$ for $KNbO_3$). Comparison of the calculated results for $q = 0.0$ in the cubic phase at 1000 K and 400 K shows a pronounced softening of the TO mode at all wavevectors. The degeneracy of the TO modes in the cubic phase is lifted in the orthorhombic phase, with one mode remaining soft and the other being greatly stiffened to about 7–8 THz. The condensation of the order parameters S_y and S_z is associated with the stiffening of the corresponding soft TO mode as shown in figure 4, which eliminates these components of the structural instability and hence the chain-like correlations along the y- and z-directions.

In an ideal displacive phase transition, a phonon frequency softens at a wavevector ($\vec{q} = 0$ in $KNbO_3$) associated with the low-temperature phase. Measurements made only near this wavevector can then suggest a purely displacive character for the transition. The fact that an entire phonon branch softens is what implies the presence of local distortions and short-range order on short length scales in real space. Thus, observations of local structure and an 'order–disorder' character can in fact be consistent with a displacive Curie–Weiss behaviour of the zone-centre optic phonon.

4. Conclusions

We have demonstrated (1) the existence in real space of chains and (2) the *dynamic* character of these chains. The MD simulations show that the chains are *preformed* well above the cubic–tetragonal phase transition temperature. The chains are defined by rows of distorted primitive cells oriented along the three cubic axes, with the atomic displacements along the chain highly correlated with one other. Displacements in different chains are uncorrelated at high temperature, and the observed phase transitions correspond to the sequential freezing or onset of coherence of families of chains along the three cubic axes. The softening of entire branches of unstable TO modes is directly associated with these real-space chains and provides a framework for understanding both the displacive and order–disorder characteristics of these phase transitions.

Acknowledgments

The work at William and Mary College was supported by Office of Naval Research grant N00014-97-1-0049. The work at Yale was supported by ONR grant N00014-97-1-0047 and the Alfred P Sloan Foundation.

References

[1] Comes R, Lambert M and Guinier A 1968 *Solid State Commun.* **6** 715
[2] Comes R, Lambert M and Guinier A 1970 *Acta Crystallogr.* A **26** 244
[3] Shapiro S M, Axe J D and Shirane G 1972 *Phys. Rev.* B **6** 4332
[4] Fontana M D, Idrissi H, Kugel G E and Wojcik K 1991 *J. Phys.: Condens. Matter* **3** 8695

[5] Teslic S, Egami T and Viehland D 1996 *J. Phys. Chem. Solids* **57** 1537
[6] Stern E A and Yacoby Y 1996 *J. Phys. Chem. Solids* **57** 1449
[7] Yu R and Krakauer H 1995 *Phys. Rev. Lett.* **74** 4067
[8] Ghosez P, Gonze X and Michenaud J-P 1998 *Ferroelectrics* **206+207** 205
[9] Rabe K M and Waghmare U V 1995 *Ferroelectrics* **164** 15
[10] Zhong W, Vanderbilt D and Rabe K M 1994 *Phys. Rev. Lett.* **73** 1861
[11] Rabe K M and Waghmare U V 1995 *Phys. Rev.* B **52** 13 236
[12] Waghmare U V and Rabe K M 1997 *Phys. Rev.* B **55** 6161
[13] Waghmare U V, Rabe K M, Krakauer H, Yu R and Wang C-Z 1998 *AIP Conf. Proc.* **436** 32
[14] Rabe K M and Waghmare U V 1997 *Ferroelectrics* **194** 118
[15] Lill J V and Broughton J 1992 *Phys. Rev.* B **46** 12 068
[16] Schneider T and Stoll E 1978 *Phys. Rev.* B **17** 1302
The spectral density $S_{\xi\xi}(q, \omega)$ is given by their equation (124).
[17] Holma M and Chen H 1996 *J. Phys. Chem. Solids* **57** 1465
[18] Krakauer H, Yu R, Wang C-Z and LaSota C 1998 *Ferroelectrics* **206+207** 133
[19] Holma M, Takesue N and Chen H 1995 *Ferroelectrics* **164** 237
[20] Hüller A 1969 *Solid State Commun.* **7** 589
Hüller A 1969 *Z. Phys.* **220** 145
[21] Fontana M D, Metrat G, Servoin J L and Gervais F 1984 *J. Phys. C: Solid State Phys.* **16** 483